IOP Publishing Nanotechnology

Nanotechnology 31 (2020) 055301 (9pp)

https://doi.org/10.1088/1361-6528/ab48bc

Additive printing of pure nanocrystalline nickel thin films using room environment electroplating

Ali Behroozfar^{1,4}, Md Emran Hossain Bhuiyan^{1,4}, Soheil Daryadel³, David Edwards², Brian J Rodriguez² and Majid Minary-Jolandan¹

E-mail: majid.minary@utdallas.ede

Received 26 July 2019, revised 3 September 2019 Accepted for publication 27 September 2019 Published 4 November 2019



Abstract

Given its high temperature stability, oxidation-, corrosion- and wear-resistance, and ferromagnetic properties, Nickel (Ni) is one of the most technologically important metals. This article reports that pure and nanocrystalline (Ni) films with excellent mechanical and magnetic properties can be additively printed at room environment without any high-temperature post-processing. The printing process is based on a nozzle-based electrochemical deposition from the classical Watt's bath. The printed Ni film showed a preferred (220) and (111) texture based on x-ray diffraction spectra. The printed Ni film had close to bulk electrical conductivity; its indentation elastic modulus and hardness was measured to be 203 ± 6.7 GPa and 6.27 ± 0.34 GPa, respectively. Magnetoresistance, magnetic hysteresis loop, and magnetic domain imaging showed promising results of the printed Ni for functional applications.

Keywords: additive printing, thin films, nanocrystalline

(Some figures may appear in colour only in the online journal)

Introduction

High temperature stability, oxidation resistance, corrosion resistance, wear resistance, and ferromagnetic properties make Nickel (Ni) an ideal metal for various applications in thin film form, for example for sensors in harsh (high temperature and corrosive) environments, and for biomedical applications [1–5]. Ni is ferromagnetic at approximately room temperature (with a Curie temperature of 358 °C), hence it is used for magnetic applications. Additionally, it is a magnetoresistive material, which means it changes its length under an applied magnetic field [6, 7]. This property makes it suitable for sensor and actuator applications. Good electrical conductivity of Ni combined with its high temperature stability make it a candidate for

microsystem products [1, 6, 8]. For such applications, Ni films are deposited using various physical and chemical processes and subsequently patterned using conventional microfabrication processes [2–5, 7]. As specific examples, electrostatic linear actuators, micromechanical switches, and Ni micro-spring for microsystem probe cards have been reported [2, 4, 5].

Recent advances in additive printing allow for direct writing of various metals in any desired patterns [9, 10]. Although additive printing of Ni is desirable, for functional applications the Ni film should be crystalline with high purity. Additive processes such as the direct ink writing and electrohydrodynamic printing may not be ideal for such purpose. Although much work has been done on additive manufacturing of Ni and its alloys at macro-scale, no additive printing of Ni thin films have been reported, so far. Such process may open up new opportunities for direct printing of

¹ Department of Mechanical Engineering, The University of Texas at Dallas, Richardson, TX 75080, United States of America

² School of Physics, University College Dublin, Belfield Dublin, Ireland

³ Department of Materials Science and Engineering, University of Illinois at Urbana-Champaign, Urbana, IL 61801, United States of America

⁴ These authors contributed equally to this work.

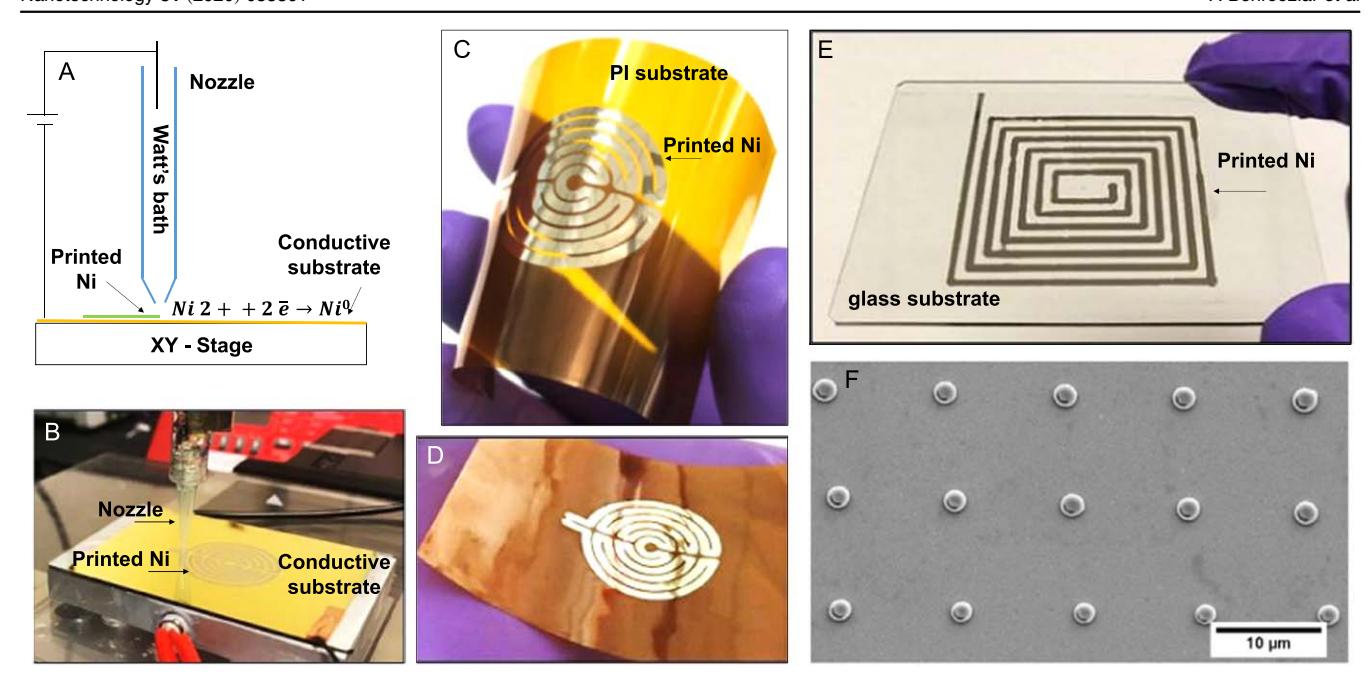


Figure 1. (A) and (B) Schematic and image of the nozzle-based Ni printing process. (C) and (D) Printed heater pattern on a flexible PI sheet. (E) Printed square spiral antenna pattern on a glass slide. (F) Ni patterns with an average diameter of ∼1500 nm printed on a substrate.

various sensors for critical applications, in particular for high temperature microelectronics and magnetic sensing.

In this article, we report additive printing of nanocrystalline Ni films at room environment (figure 1). The printing was performed using the meniscus confined electrodeposition (MCED) at the tip of a nozzle [11]. This process has been used for high quality deposition of Copper, Gold and Platinum [10, 12, 13]. We present pattering of Ni on different substrates including rigid (glass slide) and flexible (polyimide, PI) substrates. The process enables printing of high quality Ni films, with excellent mechanical, electrical and magnetic properties without need for annealing, since the process deposits crystalline metals.

The printing process is schematically shown in figure 1(A). The MCED process is based on the electroplating (electrodeposition) process. In conventional electroplating, a voltage/ current is applied between two electrodes (anode and cathode) immersed in an electrolyte bath, and metal ions are reduced and deposited on the cathode surface. In MCED, the electrolyte bath is the small liquid bridge formed between the nozzle tip and the cathode surface (substrate). A wire electrode inserted into the nozzle functions as the anode (a Ni foil in this work), and the conductive substrate functions as the cathode. The nozzle is approached to the substrate to establish an electrolyte meniscus, and this meniscus completes the ionic-electronic circuit. Printing starts when a potential/current is applied to the circuit. Ni is present in the form of divalent ions (Ni²⁺) in the electrolyte. Under current flow, positive ions react with electrons, and covert to metallic Ni⁰. Once printing is started, Ni ions are consumed and fresh electrolyte is fed into the nozzle and the liquid bridge by a syringe pump. Precise motion of positioning stages along X- and Y-directions, and the nozzle along the Z-direction results in printing of desired Ni patterns.

Since the process is a room environment process, and does not require (high temperature) annealing step, Ni can be printed on both rigid substrates (e.g. glass slide, figure 1(E)), and polymeric substrates (e.g. polyimide (PI) film, figures 1(C) and (D)). Electrochemical deposition requires a cathode for metal deposition. If the desired substrate is insulting, before printing a very thin metallic layer is deposited on the entire substrate using the electron beam-vapor deposition process. After printing, the unwanted metallic layer is etched away by a wet etching process. It is also possible to print on a nonconductive surface, if the printing starts from a conductive pad. Previous research has shown continuous printing from a conductive surface to a nonconductive surface [14]. In this case, the conductive surface functions as the initial cathode required for electroplating, and the deposition can be continued on the nonconductive surface. Additionally, we note that processes such as laser-induced selective activation can be also used to activate the polymer surface for plating.

Figures 1(C)–(E) show photographs of various printed Ni patterns. The printed patterns include a heater and a square spiral antenna. The nozzle path for making such patterns was programmed using the G-code and executed by a 3-axis controller, which controls the displacement and speed of the positioning stages. The printing was conducted under a constant current density (galvanostatic mode) of 25 mA cm⁻² (2.5 A dm⁻²) under a nozzle speed (printing speed) of 0.1 mm s⁻¹. A separate preliminary study was conducted to find the appropriate printing rate and current density. In conventional Ni plating, cathodic current density of 3-11 A dm⁻² is often used, and in which the higher current density is often achieved by increased agitation. In the MCED process, agitation similar to the conventional bath plating cannot be achieved because of limited space in the nozzle, however, rapid evaporation from the electrolyte surface contributes to the increased ionic mobility toward the nozzle tip [15–17]. Figure 1(F) shows Ni patterns with average diameter of \sim 1500 nm printed on a substrate. With downscaling the nozzle diameter, sub-micron patterns can be printed.

It can be observed that the as-printed Ni is mirror bright. The origin of brightness is not simply because of fine-grains in the deposit (to be discussed in x-ray diffraction section), but more so because of creation of flat crystals, such that the surface microstructure components form a plane from which they do not deviate by distance greater than the light wavelength [18, 19].

The line-width is controlled using the nozzle diameter. In this work, nozzle diameter in the range of \sim 0.7–1.2 mm was used. The thickness of a single print layer, based on the current density and time is on the order of several hundreds of nanometer. Depending on desired thickness, the process is repeated to obtain single or multi-layer structures. The patterns in figure 1 have three layers. In electroplating, the thickness of the Ni deposit in microns can be obtained using: thickness = $\frac{m \times 100}{\rho A}$, in which m is the amount of Ni deposited one the cathode (or dissolved at the anode) in grams, $\rho = 8.907 \,\mathrm{g \, cm^{-3}}$ is Ni density, A is the surface area to be plated. The mass can be obtained using: $m = 1.095 \times aIt$, in which the proportionality constant (1.095) in grams per amper hour equals to M/nF. M = 58.69is the atomic weight of Ni, n is the number of electrons in the electrochemical reaction (n = 2), and F is the Faraday constant. t is the time (in hours), I is the current, and a is the current efficiency (CE) ratio [19]. The anode efficiency in Ni plating is often 100%, while the cathode efficiency can vary from 90% to 97%. Discharge of hydrogen ions from water, which results in bubble formation at the cathode surface, consumes a small percentage of the current. For Ni, a = 95.5% is commonly used. The calculated CE for printed Ni in this work was obtained to be 96.0% \pm 2.3%. Details of calculation are provided in the materials and methods section.

The uniformity of the printed patterns is an important consideration. To quantify this variation, we analyzed widths and thicknesses of several printed lines and acquired zoomedin scanning electron microscopy (SEM) images of the corners. During printing, the nozzle travels a vertical line pattern in the corners, and therefore, in corners a slightly curved pattern appears, since the nozzle is circular in cross-section. We measured width and thickness on several line sections on printed lines. Overall, the variability in width and thickness was less than a few percent (obtained by standard deviation/ average ratio). The origin of such variations can be explained as following: in electroplating, the deposition rate is controlled by current density. In this work, we used the galvanostatic mode (constant current) for printing. The width of the printed line largely depends on the nozzle diameter that controls the electrolyte meniscus size at the nozzle tip. As the nozzle moves along the surface, electrolyte meniscus diameter can vary due to irregularities on the surface as well as stability of the liquid bridge of the meniscus. This in turn will result in variations in the width and thickness of the printed line. Additionally, during the printing we used a syringe pump to feed the electrolyte with a constant flow rate to the

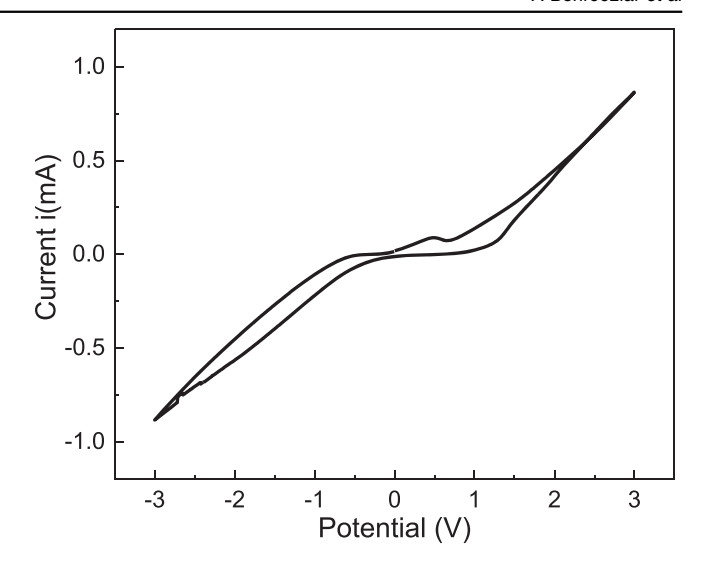


Figure 2. The cyclic voltammetry (CV) of Ni electrolyte containing 0.5 M of Nickel (II) sulfate hexahydrate, 0.1 M of Nickel (II) chloride, and 0.7 M of Boric acid in DI water. The CV response was obtained in situ (in the nozzle) at a scan rate of 10 mV s⁻¹.

meniscus zone. The pulsation of the syringe pump may also result in variations of the flow rate and meniscus diameter. Additionally, any vibrations during printing may change the meniscus geometry and hence the width and thickness of the printed lines. In this work, we did not quantify how the electrical or magnetic properties will vary with change in width and thickness. Our measurements were mostly global measurements for a section of the printed pattern. We do expect, however, that the several percentage non-uniformity would result in non-uniformity in the electrical and magnetic properties point by point. However, these variations in point by point will be averaged out over the entire printed pattern and provide average properties.

For Ni printing, the classical Watt's bath (which contains nickel sulfate, nickel chloride and boric acid) was used. Boric acid functions as the buffer, and reduces formation of cracks. Ni sulfate and Ni chloride improve the conductivity of the deposited Ni. In addition, Ni sulfate determines the limiting cathode current density, and Ni chloride improves throwing power and uniformity of the deposit. Acidity (pH) of the electrolyte has an important role on the mechanical properties of electroplated Ni. In this study, the pH of the electrolyte was kept below 4. In traditional electroplating, it has been reported that higher pH of the electrolyte results in lower quality Ni because of formation of oxides or hydroxides [20].

The electrochemical behavior of Ni electrolyte was obtained by cyclic voltammetry at the nozzle tip. Formation of hydrogen bubbles at high potential can interrupt uniform deposition process. Figure 2 shows voltammograms measured for the nozzle filled with the solution of 0.5 M of Nickel (II) sulfate hexahydrate, 0.1 M of Nickel (II) chloride, and 0.7 M of Boric acid in DI water. The voltage was swept from -3 to $3\,V$ at $10\,mV\,s^{-1}$ scan rate. The apparent oxidation peak shoulder at $\sim\!\!0.55\,V$ can be attributed to the stripping of Ni deposits.

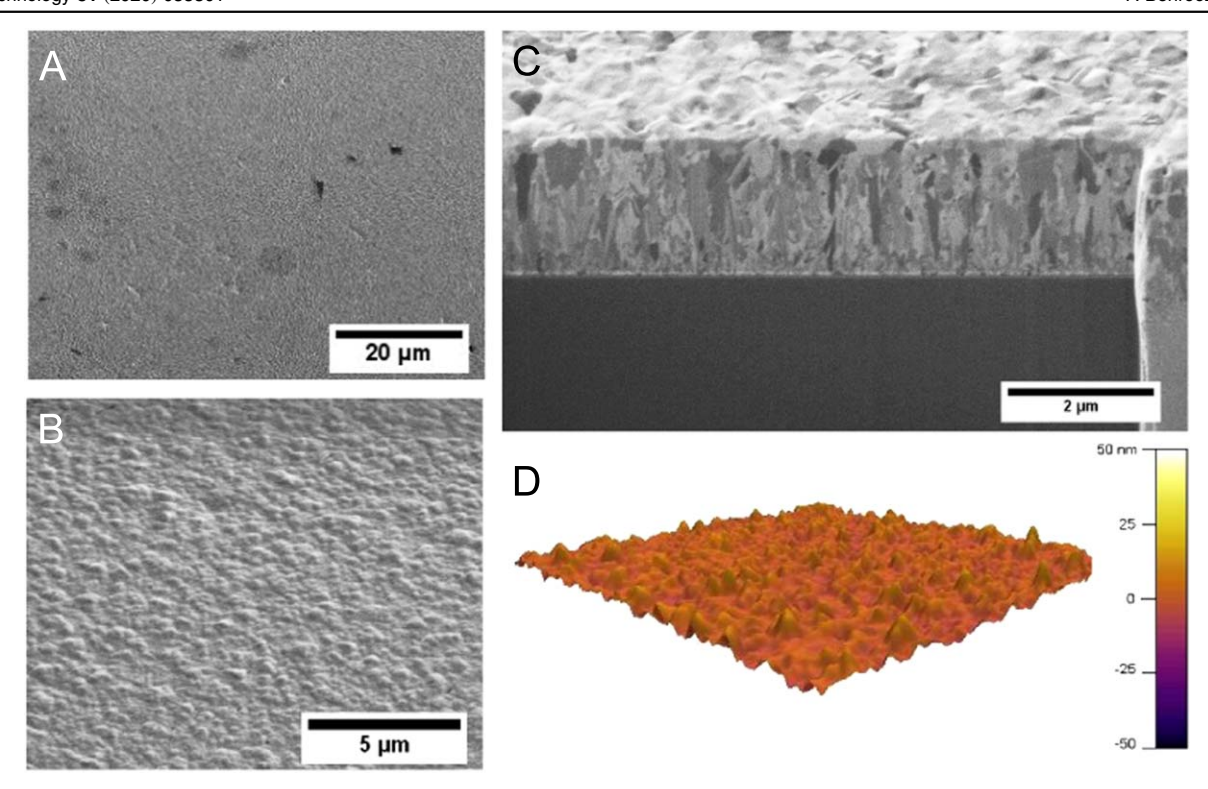


Figure 3. (A) and (B) Different magnifications SEM surface morphology images of the printed Ni. (C) FIB cross-section image of a 5-layer printed Ni. The thickness of the printed film is \sim 1.8 μ m. (D) AFM topography image of the printed Ni. Scan size is 5 μ m \times 5 μ m.

Figures 3(A) and (B) show different magnification SEM surface morphology images of the printed Ni. It can be observed that the printed Ni is continuous and uniform and with no apparent porosity. Figure 3(C) shows the focused ion beam (FIB) cross-section image of a 5-layer printed Ni. The thickness of this layer is $\sim 1.8 \,\mu \text{m}$. The FIB ion channeling contrast image shows that printed Ni is fully dense with no apparent porosity. More interestingly, the cross-section image revealed that there were no noticeable interlayer between the printed layers, as if the metal was grown epitaxially rather than layer-by-layer (five layers in this case). The presence of pores and defects degrade mechanical, electrical, and functional properties of metals, and it is known that the pores/ voids are a common problem for the layer-by-layer additive printing processes. Figure 3(D) shows a 5 μ m \times 5 μ m atomic force microscopy (AFM) surface topography image. The root mean square (rms) for this scan size is 4.9 nm.

The x-ray diffraction (XRD) spectra of the printed Ni is shown in figure 4(A). The XRD results indicate that the printed Ni is polycrystalline with face-centered cubic microstructure. The strongest peak in the XRD spectra is (220) followed by (111) peak. From (220) peak and using Scherer's equation, the estimated crystallite size is \sim 17 nm. The rms surface roughness of less than 5 nm for the printed film is another indication of nanocrystalline nature of the film (figure 3(D)).

In metal deposits, internal stresses are generated within the deposit due to electrocrystallization process and/or impurity codeposition. It is known that codeposition of sulfur results in internal compressive stress, while metal deposits from additive-free Watt's bath exhibit tensile stress in the range of 125–185 MPa [19]. To investigate the purity of the printed Ni, the energy-dispersive x-ray spectroscopy (EDS) analysis was performed. The result is shown in figure 4(B). Based on the EDS spectra, the printed Ni does not show any detectable impurity, and despite presence of different ions in the electrolyte (Watts bath), only Ni is present in the deposit.

To characterize mechanical properties of the printed Ni, nanoindentation was performed. The sample preparation and testing procedure are detailed in the materials and methods section. An array of nanoindentation footprints on printed Ni film is shown in figure 5(A), and a zoom-in image of one of the indentation marks is shown in the inset. The elastic modulus and hardness values were obtained at an indentation depth below 10% of the film thickness to avoid the substrate effects. The printed Ni has an elastic modulus and hardness of 203 ± 6.7 GPa and 6.27 ± 0.34 GPa, respectively. As a reference, the elastic modulus for bulk Ni is \sim 210 GPa. For conventional film electroplating, an elastic modulus of \sim 205 GPa has been reported for Ni [1]. Elastic modulus and the residual stress of electroplated Ni thin films have been also measured using resonance and deflection of an AFM cantilever, by plating a thin layer of Ni on the AFM cantilever. An elastic modulus in the range of 148–160 GPa was obtained. The residual stress was in the range of 32-44 MPa for Ni film thickness of $\sim 0.2-1.4 \,\mu \text{m}$ [21].

Based on the Lorentz force, a magnetic field applied on a material affects the movement of charged particles. The change in electric resistance versus the magnetic field refers to the magnetoresistance (MR) phenomenon. This phenomenon

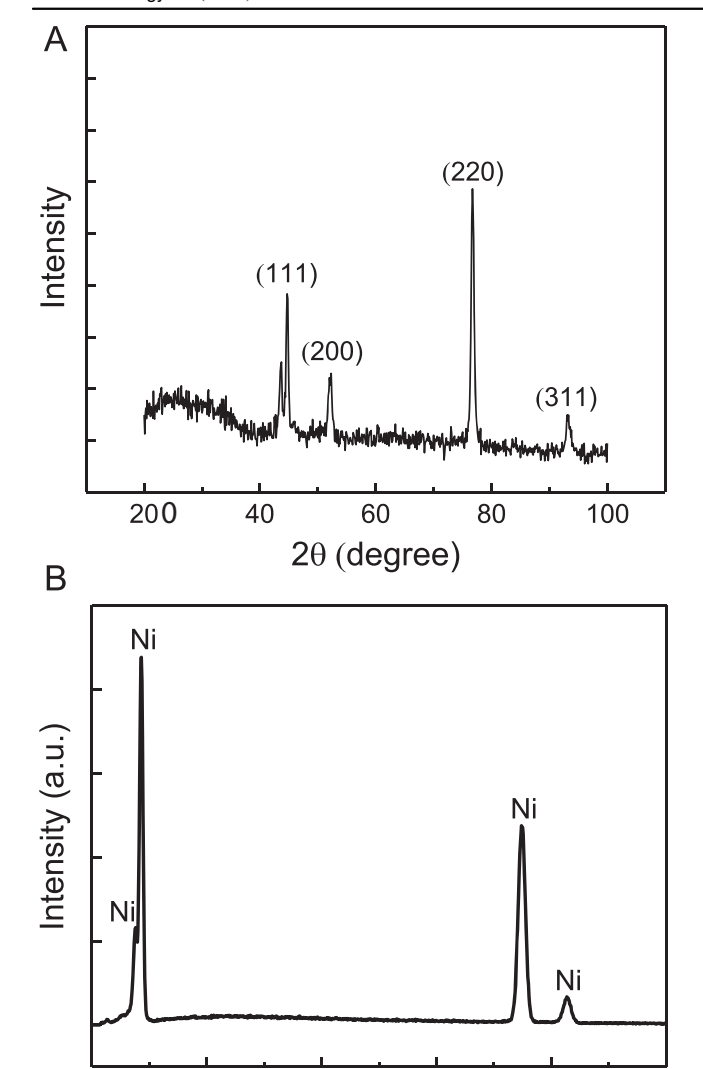


Figure 4. (A) The XRD spectra, and (B) EDS spectra of the printed Ni.

6

Energy (keV)

8

10

2

is useful for magnetic field sensing, for applications in magnetic recording, data storage, and manufacturing control processes. The phenomenon is quantified by MR ratio defined as MR ratio = $(R_0 - R_H)/R_H$, in which R_0 and R_H are the resistance in the absence and presence of an applied magnetic field, respectively. For ferromagnetic materials, the MR ratio is typically 5% or less.

MR measurements were conducted on the electroplated Ni film in the transverse mode, with the current perpendicular to the applied magnetic field. A magnetic field (up to 7 T) was applied perpendicular to the film plane and current was measured along the film plane. MR measurements showed that the resistivity of printed Ni film decreased without reaching the saturation point in the applied magnetic field range, zero to 7 T. As Ni is a well-known ferromagnetic material, this downward resistivity trend can be explained by the two theoretical models developed along with experimental validation for ferromagnetic materials by Raquet *et al* [6]. It was observed that a reduction of electron–magnon scattering

processes resulting from spin-wave damping decreases the resistivity of a ferromagnetic material under high magnetic field. The initial resistivity of the printed Ni was $9.87\times 10^{-8}~\Omega$ m, which is ${\sim}42\%$ higher than the bulk resistivity of Ni (6.99 \times $10^{-8}~\Omega$ m). In the 0–7 T magnetic field range, the plated Ni experienced ${\sim}2.28\%$ resistivity drop, which result in ${\sim}2.33\%$ MR ratio. Based on the literature, resistivity slope obtained from longitudinal MR of epitaxial Ni thin films in a $40~\mathrm{T}$ pulsed magnetic field was in the range of 0.01–0.03 $\mu\Omega$ cm T^{-1} at 300 K [6]. Another research has shown that the electroplated Ni thin film has negative resistivity slope of $-0.0161~\mu\Omega$ cm T^{-1} , MR measured in the transverse mode with an applied magnetic field up to $10~\mathrm{T}$ [8].

Figure 6(B) shows the magnetic hysteresis loop for the printed Ni thin film, which shows M (magnetization, magnetic moment per unit volume) versus H (magnetic field strength). For this measurement, the magnetic field was applied parallel to the film plane. The M-H hysteresis loops were recorded at 300 K, by varying the magnetic field from -0.4 to 0.4 T. The obtained M–H loop is symmetric. Saturation magnetization is defined as the magnetic field in which the magnetic moments of all domains are in the same direction. Measurements showed that saturation magnetization (M_s) of the printed Ni was 482.9 emu cm⁻³. The sample shows a saturation magnetization (M_s) value close to the bulk Ni (521.27 emu cm⁻³) [22]. Surface oxidation and spin disorder may create a magnetically dead layer and significantly reduce the total magnetic moment. Imperfections in the solid can also decrease the Ni saturation magnetization. The remnant magnetization (M_r) of the printed Ni was 205.33 emu cm⁻³. The M-H loop shows that the hysteresis loss is negligible.

Magnetic domains in the printed Ni film were imaged using magnetic force microscopy (MFM), figures 6(C) and (D). The MFM method is a technique based on AFM, and uses a magnetic tip to measure the magnetic force gradient distribution on a sample surface by oscillating the AFM cantilever normal to the surface at its resonant frequency, f_0 . In MFM, the tip scans the sample surface over a constant lift height (40 nm, in this case). We note that magnetic forces scale with $1/d^3$, while the van der Waals forces scale with $1/d^{\circ}$. Hence, the tip is more sensitive to magnetic forces, than van der Waals forces (which provide the topographical image) when magnetic imaging was performed at a lift height. Variations in magnetic force gradients from the sample surface cause changes in the cantilever amplitude and phase. In the MFM mode used here, the phase was maintained at 90° via a feedback loop, while the drive frequency was modulated. Figures 6(C) and (D) show the topography image and the corresponding variation in MFM frequency across regions of the film. The MFM images show bright-dark domain-like patterns with sharp contrast. The contrast is attributed to variations in the magnetic force gradient between different ferromagnetic domains, which are defined as regions of the material in which all atoms have magnetic domains in the same direction. In the MFM images, the dark regions represent the attractive force between the tip and the sample, and the light regions represent the repulsive force [23]. The

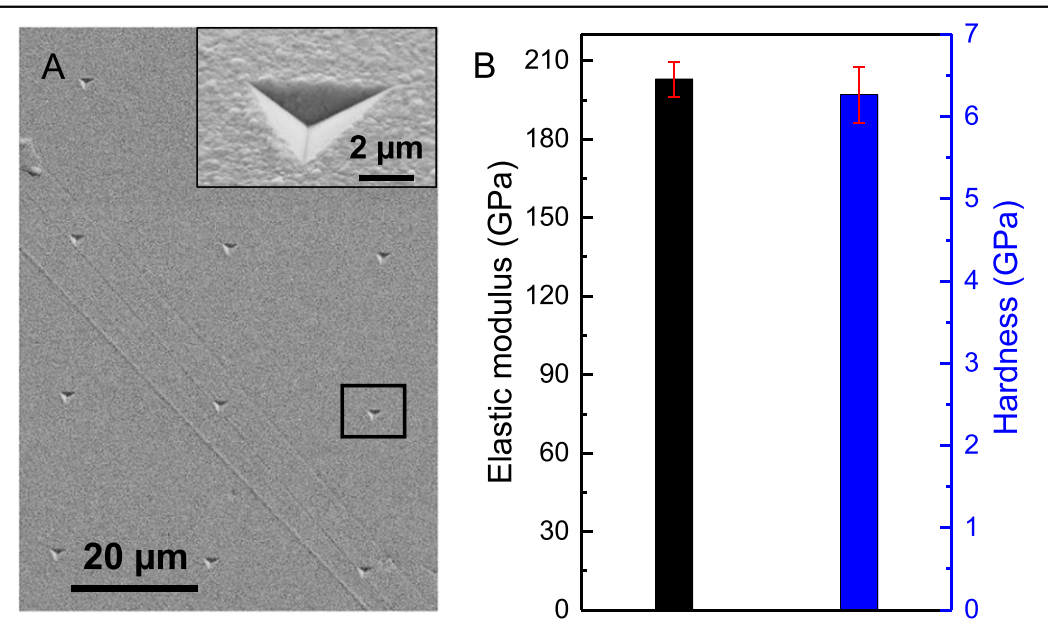


Figure 5. (A) An SEM image of an array of nanoindentation footprints on printed Ni. The inset is the zoomed-in view of one of the nanoindentation footprints. (B) The elastic modulus and hardness obtained from the nanoindentation experiment. N = 12.

magnetic domains of the printed film is obvious and ordered in the frequency shift image (figure 6(D)).

Generally, properties of Ni deposits depend on the pH, temperature, current density and chloride content of the bath. Such effects are well-documented in the literature, and it is beyond the scope of this work [3, 19]. In a separate preliminary experiment, we examined the effect of printing temperature on the properties of the printed Ni. Specifically, a heater was placed under the substrate (figure 1(B)) to bring the substrate to a set temperature of ~ 70 °C. The results showed that changes in MR and M-H loops were minimal, while Ni printed at higher temperature showed less pronounced magnetic domains in the MFM image. The deposition rate was slightly higher for the elevated temperature, such that the printed Ni had \sim 28% larger thickness. Ni printed at higher temperature had strong (111) texture, with the same purity level as the room temperature one. The crystallite size based on XRD peak was estimated to be 23 nm. Both the elastic modulus and hardness values dropped for the Ni printed at higher temperature compared to the room temperature one (elastic modulus and hardness of 113 \pm 6.9 GPa and 4.66 ± 0.56 GPa, respectively), which could be attributed to the larger grain size and different texture of the film.

Conclusions

A room environment process for additive printing of nickel thin films through scanning mode of the localized electrodeposition process was demonstrated. It is shown that high quality, mirror bright Ni can be printed in thin film form. The printed Ni is nanocrystalline, with no detectable impurities. The printed film shows electrical conductivity close to the bulk without annealing. Its mechanical properties are similar to the bulk plated Ni. In

addition, the results of MR measurement, M–H loop, and magnetic domain imaging show a great potential of the process for printing Ni for functional device applications. A potential future direction would be an investigation of various process parameters on the properties of the printed Ni to obtain optimal parameters for specific applications.

Materials and methods

Materials

The classical Watt's bath was used as the electrolyte solution to print Ni. The electrolyte was composed of 0.5 M of Nickel (II) sulfate hexahydrate (Sigma-Aldrich), 0.1 M of Nickel (II) chloride (Sigma-Aldrich) and 0.7 M of Boric acid (Sigma-Aldrich) in DI water. The anode was a Nickel foil (40 mm \times 10 mm \times 0.5 mm with a purity of %99.98, Sigma-Aldrich), which was inserted into the plastic syringe nozzle. The printing substrates (cathode) were a glass slide or a 50 μm thick polyimide (PI) foil (Kapton 50HN by DuPont) coated by 30 nm of Gold or Nickel. Ni etchant (TFG type from TRANSENE) consisting of less than 1% Thiourea, 10%-15% Sodium n-nitrobenzene sulfonate, less than 10% sulfuric acid, and more than 75% water by weight was used to etch the conductive coating after printing, when necessary.

The printer setup

Plastic pipette tips with diameters of 1.2 or 0.7 mm were used as printing nozzles. The pipette tip was mounted on a 1 ml plastic syringe, which was used to keep electrolyte and Nickel foil (Anode). Through a plastic tube, the 1 ml syringe was connected to a larger syringe (20 ml) mounted on a syringe pump (NE-300 New Era Pump). Using this system, the electrolyte

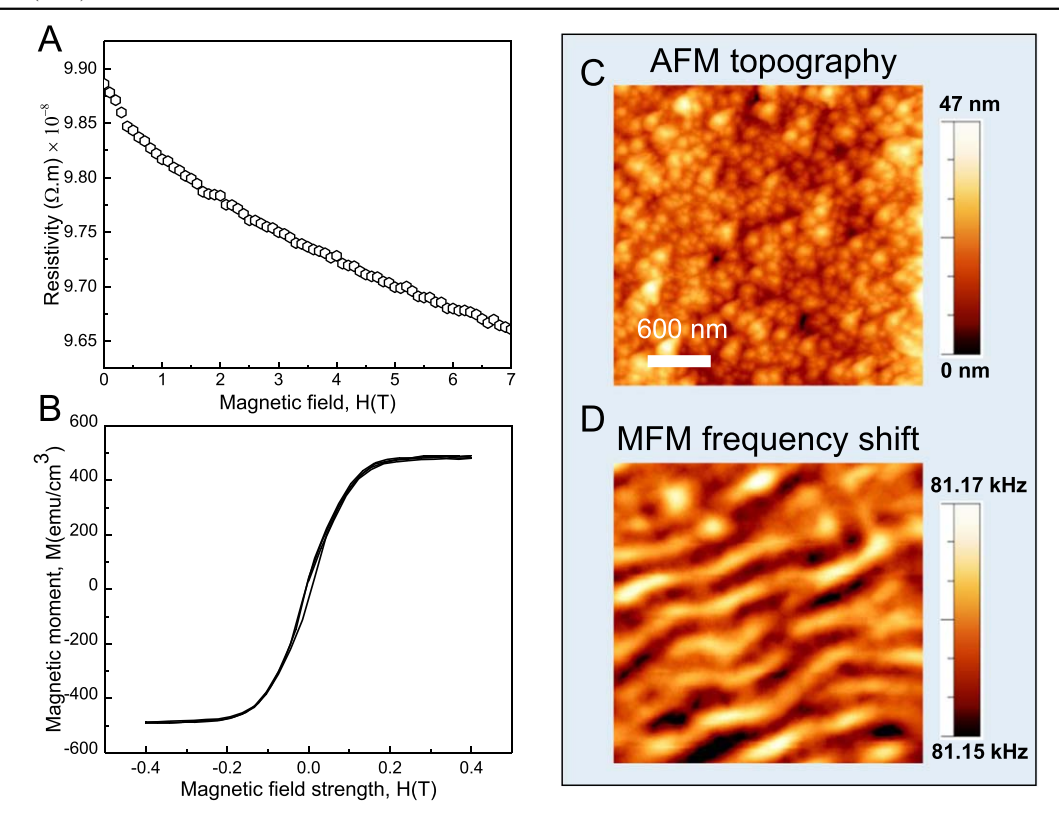


Figure 6. (A) The magnetoresistance behavior of the printed Ni film. (B) The magnetic hysteresis loop of printed Ni with the magnetic field applied parallel to the film plane. (C) and (D) Surface topography AFM image and the corresponding magnetic domain structures based on MFM frequency shift, respectively. Each image is $3 \mu m \times 3 \mu m$ in size.

was fed to the printing area during the process. The 1 ml syringe was moved by a motorized linear stage (150 mm displacement range, Newport) along the Z-axis during the printing. The substrate was placed on an XY motorized linear stage (150 mm displacement range, Newport). Movement along the x, y, and z directions was controlled simultaneously using a controller based on the printing paths programmed by G-code for each specific pattern. When required, a heating stage was placed on the x-y stage just below the substrate to facilitate printing at higher temperature. The heating stage was an aluminum plate (75 mm \times 50 mm \times 10 mm) with a heater and thermocouple inserted into it to monitor the temperature of the heater plate. The deposition current was provided by a VersaSTAT-4 Potentiostat/Galvanostat (Princeton Applied Research).

Functional device fabrication

A <30 nm conductive Ni layer was deposited by using an e-beam vapor deposition system at a base pressure better than 5×10^{-6} Torr with a deposition rate of 0.4 angstrom s⁻¹. The substrate was ultrasonically cleaned with acetone and isopropanol before putting in the e-beam vapor deposition chamber. The current density was maintained at 25 mA cm⁻² (2.5 A dm⁻²) for Ni printing, and the nozzle speed (printing speed) was set to 0.1 mm s⁻¹. All the mentioned parameters for Ni printing at this scale were achieved after a set of preliminary experiments and microscopic analysis. To remove the e-beam vapor deposited Ni, wet etching was performed using Ni etchant. As Ni etchant works faster at elevated

temperatures, Ni etching was performed at 50 °C for approximately 90 s to remove the 30 nm Ni layer.

The CE calculation

To calculate the CE of the Ni printing, the theoretical thickness of the 5-layer Ni printed line was obtained using $S = \frac{m \times 100}{\rho A}$, in which m is amount of Ni deposited at the cathode in grams, $\rho = 8.907$ g cm $^{-3}$ is Ni density, A is the surface area to be plated in dm 2 . The mass (m) was calculated using: $m = 1.095 \times aIt$, in which the proportionality constant (1.095) in grams per amper hour equal to M/nF. M = 58.69 is the atomic weight of Ni, n is the number of electrons in the electrochemical reaction (n = 2), and F is the Faraday constant (26.799 A-h). a is the CE ratio (used a = 1, when theoretical calculation was done), t is the time in hours to print five lines, and t is the applied current in Amper. Several profilometer scans were taken to get the average actual thickness of the 5-layer Ni printed line. The actual thickness was divided by the theoretical value to get the CE.

Ion channeling contrast image

A dual beam FEI NOVA 200 FIB was used to make cross-sections on the samples and acquire ion channeling contrast images after cutting and polishing the cross-section. Each cross-section was made in several steps using beam voltage of 30 kV and three different currents including high current (5 nA), medium current (1 nA), and low current (0.1 nA). Ion channel images were acquired using low energy ion beam (30 KV, 10 pA).

XRD sample preparation and experiment

The crystal structure of the printed Ni was studied by XRD. A $10 \, \mathrm{mm} \times 10 \, \mathrm{mm}$ size (consisting of 10 overlaying lines in 5 layers) sample was printed on a Si wafer. XRD measurements were performed in a Rigaku smartlab XRD using a Cu K α radiation with a wavelength of $\lambda = 0.154\,06\,\mathrm{nm}$ in the range of $2\theta = 20^\circ - 100^\circ$. Scanning step size and speed were Δ $(2\theta) = 0.01^\circ$ and 1 deg min⁻¹, respectively. The voltage and current were set at $40\,\mathrm{kV}$ and $44\,\mathrm{mA}$, respectively.

EDS sample preparation and experiment

The elemental analysis was conducted using a ZEISS supra 40 scanning electron microscope (SEM). In this regard, multilayer lines (consisting of 30 layers) of Ni were printed at room temperature and 70 °C. The multi-layer lines were thick enough to avoid detection of the substrate composition by EDS. The EDS analysis was done at least three times at different points for each sample.

Nanoindentation

5-layer samples were printed on Si wafer at both room temperature and elevated temperature for the nanoindentation experiment. Roughness of the sample surface was measured by an AFM, MFP-3D-BIO (Asylum Research) to estimate the approximate required indentation depth. The nanoindentation tests were performed using a NanoFlip nanoindenter (Nanomechanics, Inc.) equipped with a Berkovich tip. 45-50 mN load was applied with an indentation strain rate of $0.05 \,\mathrm{s}^{-1}$. The indentation depth was predetermined less than 10% of the thickness of Ni film. The elastic modulus and hardness versus the indentation depth were obtained directly from the nanoindenter software. In the system, the continuous stiffness measurement (CSM) technique was used to determine the hardness and modulus of elasticity versus the indentation depth [24]. CSM involves a harmonic oscillating force and the displacement response of the indenter tip. The CSM technique measures the contact stiffness at any point on the loading curve, and on the unloading curve.

AFM and MFM sample preparation and experiment

The surface roughness analysis and magnetic domain structures imaging were performed using an Asylum MFP-3D-BIO AFM. Ni line patterns were printed on a gold-coated Si wafer. To obtain the rms value of the surface roughness, and rms value of the frequency change due to the magnetic force, at least three scans were performed for each sample at different locations. AFM images were recorded over scan area of $3 \, \mu \mathrm{m} \times 3 \, \mu \mathrm{m}$ with a resolution of 512×512 pixels. Prior to the experiment, the Co–Cr coated MFM tip was magnetized approximately in the out-of-plane direction. All the MFM images were obtained at the same lift scan height of 40 nm, using the lift mode at room temperature.

MR sample preparation and experiment

Physical property measurement system (PPMS) (Model 6000) by quantum design was employed to measure the resistance change with respect to magnetic field. The magnetic field was applied perpendicular to the current flow in the printed line. A 10 mm linear Ni line with 10 layers was printed on a coppercoated Si wafer. After printing, the entire substrate was etched to remove the initial deposited Cu from the unprinted part. Four probes connection was made to measure the resistance change continuously with respect to the magnetic field change. The resistance of the 30 nm deposited initial Cu layer under the printed line was subtracted from the total resistance. To subtract the resistance of the initial e-beam deposited layer, we considered the printed line and the evaporated line as two resistors connected in parallel, and the parallel resistance $\left(\frac{1}{R_{total}} = \frac{1}{R_{LED \, process}} + \frac{1}{R_{e-beam \, process}}\right)$ equation was used to obtain the resistance of the printed line by printing process. No resistance change was considered for copper, since it does not have magnetic property.

Magnetic hysteresis experiment and sample preparation

Magnetic hysteresis loops were measured by a PPMS (Model 6000) with the maximum applied field of 3 T parallel to the length direction of printed Ni. The measurement temperature was maintained at 300 K. A $10\,\mathrm{mm}\times10\,\mathrm{mm}$ size sample (consisting of 10 overlaying lines in 5 layers) was printed on Cu coated polyimide (PI) sheet for both conditions, room temperature, and $70\,^{\circ}\mathrm{C}$.

Acknowledgments

This work was supported by the US National Science Foundation (NSF-CMMI, award # 1727539) and The US Office of Naval Research (ONR, award # N00014-15-1-2795). Support for DE and BJR was provided in part by a research grant from Science Foundation Ireland (SFI) and the Sustainable Energy Authority of Ireland (SEAI) under the SFI Career Development Award Grant Number SFI/17/CDA/4637 and the US-Ireland R&D Partnership Program Grant Number SFI/14/US/I3113.

ORCID iDs

David Edwards https://orcid.org/0000-0002-9480-4936
Brian J Rodriguez https://orcid.org/0000-0001-9419-2717
Majid Minary-Jolandan https://orcid.org/0000-0003-2472-302X

References

- [1] Luo J *et al* 2004 Young's modulus of electroplated Ni thin film for MEMS applications *Mater. Lett.* **58** 2306–9
- [2] Matsunaga T et al 2000 Fabrication of a new electrostatic linear actuator Jpn. J. Appl. Phys. 39 7115–9

- [3] Luo J et al 2006 Effects of process conditions on properties of electroplated Ni thin films for microsystem applications J. Electrochem. Soc. 153 D155–61
- [4] Kataoka K et al 2004 Contact properties of Ni micro-springs for MEMS probe card Proc. 50th IEEE Holm Conf. on Electrical Contacts and the 22nd Int. Conf. on Electrical Contacts Electrical Contacts, 2004
- [5] Teh W H et al 2003 Near-zero curvature fabrication of miniaturized micromechanical Ni switches using electron beam cross-linked PMMA J. Micromech. Microeng. 13 591–8
- [6] Raquet B et al 2002 Electron-magnon scattering and magnetic resistivity in 3 d ferromagnets Phys. Rev. B 66 024433
- [7] Yi J B et al 2004 An investigation of structure, magnetic properties and magnetoresistance of Ni films prepared by sputtering J. Magn. Magn. Mater. 284 303–11
- [8] Boye S A, Lazor P and Ahuja R 2005 Magnetoresistance and Halleffect measurements of Ni thin films J. Appl. Phys. 97 083902
- [9] Hirt L *et al* 2017 Additive manufacturing of metal structures at the micrometer scale *Adv. Mater.* **29** 1604211
- [10] Behroozfar A et al 2018 Microscale 3D printing of nanotwinned copper Adv. Mater. 30 1705107
- [11] Hu J and Yu M-F 2010 Meniscus-confined three-dimensional electrodeposition for direct writing of wire bonds *Science* 329 313–6
- [12] Suryavanshi A P and Yu M-F 2007 Electrochemical fountain pen nanofabrication of vertically grown platinum nanowires *Nanotechnology* 18 105305
- [13] Daryadel S, Behroozfar A and Minary-Jolandan M 2019 Toward control of microstructure in microscale additive manufacturing of copper using localized electrodeposition Adv. Eng. Mater. 21 1800946
- [14] Lei Y *et al* 2018 Dynamic 'scanning-mode' meniscus confined electrodepositing and micropatterning of individually

- addressable ultraconductive copper line arrays *J. Phys. Chem. Lett.* **9** 2380–7
- [15] Morsali S et al 2017 Multi-physics simulation of metal printing at micro/nanoscale using meniscus-confined electrodeposition: effect of nozzle speed and diameter J. Appl. Phys. 121 214305
- [16] Morsali S et al 2017 Multi-physics simulation of metal printing at micro/nanoscale using meniscus-confined electrodeposition: Effect of environmental humidity J. Appl. Phys. 121 024903
- [17] Morsali R, Qian D and Minary-Jolandan M 2019 Mechanisms of localized pulsed electrodeposition (L-PED) for microscale 3D printing of nanotwinned metals J. Electrochem. Soc. 166 D354–8
- [18] Weil R and Paquin R 1960 The relationship between brightness and structure in electroplated nickel *J. Electrochem. Soc.* **107** 87–91
- [19] Schlesinger M and Paunovic M 2011 *Modern Electroplating* (New York: Wiley)
- [20] Wang X W et al 2005 Size-dependent orientation growth of large-area ordered Ni nanowire arrays J. Phys. Chem. B 109 24326–30
- [21] Kim S-H 2007 Determination of mechanical properties of electroplated Ni thin film using the resonance method *Mater*. *Lett.* 61 3589–92
- [22] Wohlfarth E 1980 Iron, cobalt and nickel Handbook of Ferromagnetic Materials vol 1 (Amsterdam: Elsevier) pp 1–70
- [23] Kazakova O et al 2019 Frontiers of magnetic force microscopy J. Appl. Phys. 125 060901
- [24] Hay J, Agee P and Herbert E 2010 Continuous stiffness measurement during instrumented indentation testing *Exp. Tech.* 34 86–94